PAPER

Blind Signal Separation for Array Radar Measurement Using Mathematical Model of Pulse Wave Propagation

Takuya SAKAMOTO[†,††a)], ***Member***

SUMMARY This paper presents a novel blind signal separation method for the measurement of pulse waves at multiple body positions using an array radar system. The proposed method is based on a mathematical model of pulse wave propagation. The model relies on three factors: (1) a small displacement approximation, (2) beam pattern orthogonality, and (3) an impulse response model of pulse waves. The separation of radar echoes is formulated as an optimization problem, and the associated objective function is established using the mathematical model. We evaluate the performance of the proposed method using measured radar data from participants lying in a prone position. The accuracy of the proposed method, in terms of estimating the body displacements, is measured using reference data taken from laser displacement sensors. The average estimation errors are found to be 10–21% smaller than those of conventional methods. These results indicate the effectiveness of the proposed method for achieving noncontact measurements of the displacements of multiple body positions.

key words: *array radar, blind signal separation, mathematical model, pulse wave propagation*

1. Introduction

According to a survey conducted by the National Center for Health Statistics in the United States, 30.3 million adults were diagnosed with heart disease in 2018 [1]. Some heart diseases are associated with the progression of hypertension and atherosclerosis [2]. Therefore, it is important to establish a simple and noninvasive approach for the long-term monitoring of the condition of blood vessels to enable early diagnosis of such diseases.

A pulse wave is an elastic wave that propagates to the periphery of the body as the heart contracts. The pulse arrival time (PAT), pulse transit time (PTT) and pulse wave velocity (PWV) are known to be predictors of arterial stiffness and related cardiovascular diseases [2]–[8]. The PWV is expressed by the Moens–Korteweg equation $v_{\mathrm{PWV}} = \sqrt{Ea/2r\rho}$, where E is Young's modulus, a is the thickness of the arterial wall, r is the radius of the artery, and ρ is the blood density. This equation indicates that a stiffer arterial wall will produce a higher PWV [9]. To estimate the PTT/PWV, it is necessary to measure pulse waves simultaneously at multiple body positions.

Manuscript received October 10, 2021.
Manuscript revised January 8, 2022.
Manuscript publicized February 18, 2022.

[†]The author is with the Department of Electrical Engineering, Graduate School of Engineering, Kyoto University, Kyoto-shi, 615-8510 Japan.
[††]The author is also with Japan Science and Technology Agency, PRESTO, Kawaguchi-shi, 332-0012 Japan.
a) E-mail: sakamoto.takuya.8n@kyoto-u.ac.jp
DOI: 10.1587/transcom.2021EBP3167

Many conventional studies on the measurement of the PTT/PWV involve the use of contact-type sensors [10]–[15]. McCombie et al. [16] reported the estimation of the PWV by measuring pulse wave signals using two photoplethysmography (PPG) sensors placed on the wrist and fingers. Hsu et al. [17] measured the PWV by placing two microelectromechanical systems in close proximity to the wrist/neck, while Holz et al. [18] used smart glasses with three built-in PPG sensors to measure the PTT. Other studies [19]–[21] have measured the PTT using PPG, ballistocardiography, electrocardiography (ECG), and impedance cardiography (ICG) sensors.

Contact-type sensors are, however, not suitable for the long-term monitoring of pulse waves and arterial status. Noncontact measurements using a radar system represent a promising alternative for determining the PTT/PWV. Buxi et al. [22] estimated the PTT using a 1-GHz microwave radar along with ECG, ICG, and phonocardiogram sensors. They also measured the PTT using a 1.1-GHz radar with ECG and bioimpedance data [23]. Ebrahim et al. [24] estimated the PTT using a 900-MHz continuous wave radar with ECG and PPG sensors, and Kuwahara et al. [25] estimated the PWV using a 2.4-GHz radar system and piezoelectric sensors. These studies used contact sensors in addition to radar, and so they are not suitable for long-term monitoring.

Several studies have reported PTT/PWV measurements obtained using only radar systems, i.e., without any contact-type sensors [26]–[28]. Lu et al. [26] reported the measurement of the PWV using two radar systems (6.05 and 5.63 GHz), while Michler et al. [27] determined the PWV by simultaneously measuring the displacements of two positions on the abdomen using a 24-GHz phased-array radar system. The techniques used in these studies require the target body positions as prior information, which means they cannot be applied without knowing the actual position and posture of the target person in advance.

Previous studies by the author [29], [30] reported a technique that uses a single-array radar system for the measurement of pulse wave propagation and does not require prior information about the positions of target body parts. Using the single-array radar system, one previous study [29] measured the body displacements caused by pulse waves in the back and calf of the target person. In this previous study, a conventional beamformer (BF) method was used to discriminate the radar echoes from multiple body parts, but this approach has an obvious limitation regarding the dependency of the angular resolution on the array aperture size.

To analyze the body displacements at multiple positions in proximity, a high-resolution method is required. When estimating a PTT value, it is advantageous to measure multiple body positions in proximity because the body displacement waveforms are, in many cases, highly correlated when the measured positions are close to each other; the displacement waveforms of pulse waves often become distorted after long-distance propagation.

To attain high-resolution signal discrimination, the author later proposed a blind signal separation method based on a simplified mathematical model of the body displacements caused by pulse waves [30]. This method, called physiological component analysis (PHCA), is based on the optimization of an objective function comprising the small displacement approximation and a simplified impulse response function. Although the method is effective in numerical simulations assuming a simplified model, its applicability to measured data has not yet been established.

The purpose of this study is to develop a new blind signal separation method for the discrimination of radar echoes using a precise mathematical model of pulse wave propagation. More specifically, inspired by the impulse response waveforms presented in [29], we modify the objective function of PHCA [30] using the proposed mathematical model. The newly introduced objective function is calculated from the approximate residuals between the impulse response waveforms obtained from the measured data and the proposed mathematical model. The proposed method is applied to experimental data obtained from two participants, and its accuracy is evaluated and compared with that of existing methods.

2. Conventional Signal Separation Methods Using Array Radar

2.1 Array Signal Model and Signal Separation

We assume that the radar receives echoes from multiple body positions. Let $d_n(t)$ be the skin displacement waveform at the n-th body position ($n = 1, \cdots, N$), and denote the body displacement vector by $\boldsymbol{d}(t) = [d_1(t), d_2(t), \cdots, d_N(t)]^{\mathrm{T}}$. We assume that the echo from the n-th body position is phase-modulated by the displacement $d_n(t)$ as $s_n(t) \propto \mathrm{e}^{\mathrm{j}2kd_n(t)}$, where k is the wave number. The echo vector is denoted by $\boldsymbol{s}(t) = [s_1(t), s_2(t), \cdots, s_N(t)]^{\mathrm{T}} = \exp(\mathrm{j}2k\boldsymbol{d}(t))$. The received signal vector $\boldsymbol{x}(t)$ is defined as $\boldsymbol{x}(t) = [x_1(t), x_2(t), \cdots, x_M(t)]^{\mathrm{T}}$, where $x_m(t)$ is the signal received from the m-th element and $N \leq M$ is assumed. We assume that the received signal vector $\boldsymbol{x}(t)$ is expressed as $\boldsymbol{x}(t) = A\boldsymbol{s}(t) + \boldsymbol{n}(t)$, where A is an $M \times N$ mixing matrix and $\boldsymbol{n}(t)$ is an additive noise vector. If an unmixing matrix W is given, the mixed signals can be properly separated according to $\hat{\boldsymbol{s}}(t) = W\boldsymbol{x}(t)$, and the displacement can be estimated as $\hat{\boldsymbol{d}}(t) = (1/2k)\angle\hat{\boldsymbol{s}}(t)$. The following section describes a method for estimating the optimum weight matrix W that separates the echoes and restores the body displacement waveforms. Fig. 1 shows a system model with an array radar system for measuring $M = 2$ body positions.

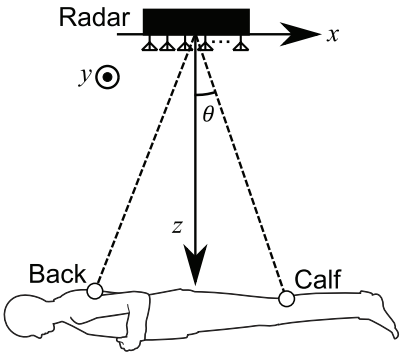

Fig. 1 System model of measurement of pulse wave propagation using array radar system.

2.2 Physiological Component Analysis

This section reviews the conventional blind signal separation method of PHCA, which is based on a mathematical model of body displacements caused by pulse wave propagation. In PHCA, signal separation is formulated as an optimization problem using the product of four different functions (i.e., $F(W) = F_1(W)F_2(W)F_3(W)F_4(W)$) as the objective function [30]. Signal separation is achieved in the form of the optimization problem $\max_W F(W)$. The components of the objective function, $F_1(W)$, $F_2(W)$, $F_3(W)$, and $F_4(W)$, are derived from three approximations, which are explained as follows.

2.2.1 Small Displacement Approximation

We assume that body displacements are sufficiently smaller than the wavelength, which allows us to approximate the I-Q plot of each separated echo moving along a straight line. This approximation can be interpreted as the condition number of the covariance matrix R_m of the real and imaginary parts of $\hat{s}_m(t)$, i.e.,

$$R_m = \int_{-\infty}^{\infty} \begin{pmatrix} \mathrm{Re}[\hat{s}_m(t)]^2 & \mathrm{Re}[\hat{s}_m(t)]\mathrm{Im}[\hat{s}_m(t)] \\ \mathrm{Re}[\hat{s}_m(t)]\mathrm{Im}[\hat{s}_m(t)] & \mathrm{Im}[\hat{s}_m(t)]^2 \end{pmatrix} \mathrm{d}t. \tag{1}$$

The condition number is given as $\kappa(R_m) = |\lambda_{\max}/\lambda_{\min}|$, where $\lambda_{\max}$ and $\lambda_{\min}$ are the larger and smaller eigenvalues of R_m, respectively. When the I-Q plot of $\hat{s}_n(t)$ forms a straight trajectory, $\kappa(R_m)$ is large, and this is exploited to derive function $F_1(W)$ as

$$F_1(W) = \min_{1 \leq m \leq M} \lambda_m^{\beta}, \tag{2}$$

where λ_m is defined as [30]

$$\begin{aligned} \lambda_m^2 = &\left| \int_{-\infty}^{\infty} \left(\mathrm{Re}[\hat{s}_m(t)]^2 - \mathrm{Im}[\hat{s}_m(t)]^2 \right) \mathrm{d}t \right|^2 \\ &+ 4 \left| \int_{-\infty}^{\infty} \mathrm{Re}[\hat{s}_m(t)]\mathrm{Im}[\hat{s}_m(t)] \, \mathrm{d}t \right|^2 . \end{aligned} \tag{3}$$

2.2.2 Beam Pattern Orthogonality Approximation

The optimized unmixing matrix $W = [\boldsymbol{w}_1, \boldsymbol{w}_2, \cdots, \boldsymbol{w}_N]^{\mathrm{T}}$ comprises N weight vectors $\boldsymbol{w}_n^{\mathrm{T}}$ $(n = 1, \cdots, N)$. Ideally, each weight vector forms a beam pattern in which the mainlobe is approximately directed towards the target and several nulls are directed towards other interfering targets. Therefore, we can assume the orthogonality of the beampatterns for the weight vectors. Let the beampattern of the n-th weight vector be

$$\boldsymbol{b}_n = (Q_{\mathrm{DFT}}\boldsymbol{w}_n) \circ (Q_{\mathrm{DFT}}\boldsymbol{w}_n)^*, \tag{4}$$

where $\circ$ denotes the element-wise multiplication operator and Q_{DFT} is a discrete Fourier transform matrix. We derive a function $F_2(W)$ that takes a large value when the orthogonality condition holds as follows:

$$F_2(W) = \prod_{1 \le i < j \le M} \min\left\{(\boldsymbol{b}_i^{\mathrm{T}}\boldsymbol{b}_j)^{-1}, \gamma\right\}, \tag{5}$$

where γ is a constant.

2.2.3 Simplified Impulse Response Model of Pulse Wave Propagation

Pulse waves propagate from the heart toward the periphery of the body. The simplest model of pulse wave propagation uses a constant multiple of a time-shifted template waveform. The n-th body displacement waveform $d_n(t)$ is approximated as

$$d_n(t) \simeq \alpha_n d_0(t - \tau_n), \tag{6}$$

where α_n is a constant, $d_0(t)$ is the template waveform, and τ_n corresponds to the propagation delay. Using Dirac's delta function $\delta(t)$, (6) can be described as

$$d_n(t) = d_0(t) * \alpha_n \delta(t - \tau_n), \tag{7}$$

where $*$ denotes the convolution integral. The impulse response $\hat{h}_{i,j}(t)$ between the i-th and j-th body positions is calculated from the deconvolution of the estimated displacement waveforms $\hat{d}_i(t)$ and $\hat{d}_j(t)$. The functions $F_3(W)$ and $F_4(W)$ are given by

$$F_3(W) = \prod_{1 \le i < j \le M} \frac{\int |h_{i,j}(t)|^4 \, \mathrm{d}t}{\left(\int_{-\infty}^{\infty} |h_{i,j}(t)|^2 \, \mathrm{d}t\right)^2} \tag{8}$$

and

$$F_4(W) = \prod_{1 \le i < j \le M} \frac{\max_{t>0} |\hat{h}_{i,j}(t)|^2}{\max_{t<0} |\hat{h}_{i,j}(t)|^2}. \tag{9}$$

Note that $F_3(W)$ takes a large value when the nonzero components are concentrated, which means that $\hat{h}_{i,j}(t)$ is close to a delta function. Additionally, note that $F_4(W)$ takes a large value when the causality holds, which means that $\hat{h}_{i,j}(t)$ only has nonzero components for $t > 0$.

3. Proposed Blind Signal Separation Method Using Array Radar

3.1 Refined Mathematical Model of Impulse Response of Pulse Wave Propagation

In this section, we revise the objective function $F(W)$ of conventional PHCA based on a refined mathematical model of pulse wave propagation, thus improving the accuracy of the separation of radar echoes. The simplified pulse propagation model used for PHCA results in the functions $F_3(W)$ and $F_4(W)$. The application of PHCA using these functions is effective to some extent for signal separation [30]. However, the question remains of whether a better mathematical model, which is more realistic and reflects the actual data, exists.

To answer this question, we measured the human body displacement waveforms using laser displacement sensors instead of radar systems. Two laser displacement sensors were placed at a distance of 150 mm from the skin surface of the back and calf of two participants. The experimental setup is shown in Fig. 2. The parameters of the laser displacement sensors are listed in Table 1. The biometric information of the participants is summarized in Table 2.

Displacement waveforms $d_1(t)$ and $d_2(t)$ were measured at the back and calf, respectively (see Fig. 2). The impulse responses $h_{1,2}(t)$ were then estimated using deconvolution, which was approximated using the Wiener filter. The same measurements were repeated for both participants (A and B). As an example, the measured displacement waveforms $d_1(t)$ and $d_2(t)$ of participant A are shown in Fig. 3. In the figure,

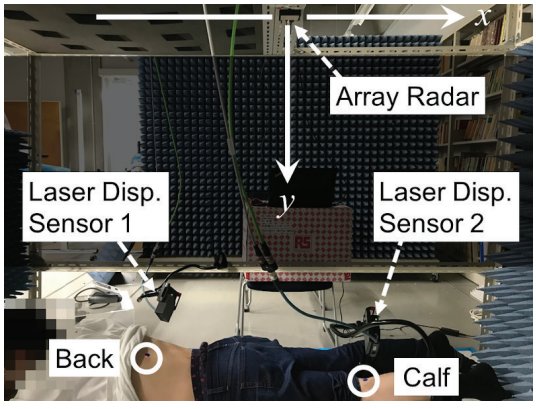

Fig. 2 Measurement setup using an array radar system and laser displacement sensors.

Table 1 Parameters of the laser displacement sensors.

Measurement principle	Triangulation
Measurable distance	150 ± 40 mm
Spot size (diameter)	120 μm
Repeatability	0.2 μm
Wavelength	655 nm
Sampling interval	500 μs

Table 2 Biometric information of participants.

Participant	A	B
Age	23	22
Sex	M	M
Weight (kg)	55	53
Height (cm)	166	169
BMI (kg/m^2)	20.0	18.6
Blood pressure (mmHg)	115/80	111/77
Heart rate (bpm)	63	58

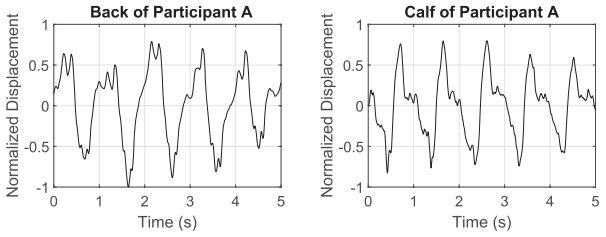

Fig. 3 Displacement waveforms of the back $d_1(t)$ (left) and the calf $d_2(t)$ (right) of participant A measured using laser displacement sensors.

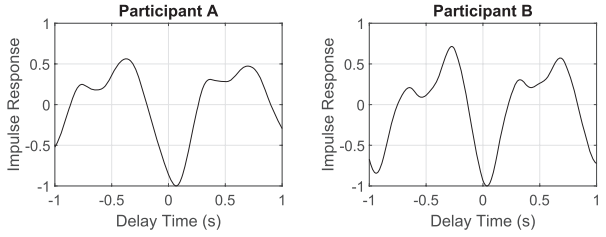

Fig. 4 Impulse responses of pulse waves measured using laser displacement sensors for participants A (left) and B (right).

the waveforms appear to be quite different. Note that the pulse wave propagation is not simply a constant multiple of a time-shifted waveform, and so a new mathematical model must be incorporated in the optimization objective function. The estimated impulse responses $h_{1,2}(t)$ are shown in Fig. 4 for participants A and B. The impulse responses appear complicated; they cannot be accurately modeled using only a delta function. The impulse response has a trough at $t = 0.04$ s for participant A and at $t = 0.07$ s for participant B. The trough is followed by double peaks, located at $t = 0.33$ s and 0.68 s for participant A and at $t = 0.37$ s and 0.70 s for participant B.

3.2 Objective Function Using Refined Mathematical Model of Pulse Wave Propagation

In this section, we propose a mathematical model of pulse wave propagation, and use the model to derive a new objective function for the optimization problem. The model must be sufficiently flexible to express various curves with individual differences. We propose a model function $g_{\boldsymbol{p}}(t)$ defined as

$$g_{\boldsymbol{p}}(t) = -g_0 \left\{ \cos\left(\omega(t - t_0)\right) + \alpha \cos\left(2\omega(t - t_0) + \phi\right) \right\}, \tag{10}$$

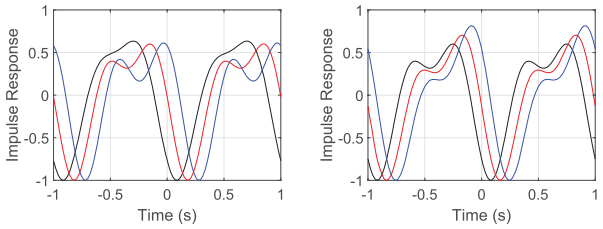

Fig. 5 Proposed model function examples for $\boldsymbol{p} = [\omega_0, \alpha_1, t_1, \phi_1]$ (black), $[\omega_0, \alpha_2, t_2, \phi_1]$ (red), and $[\omega_0, \alpha_3, t_3, \phi_1]$ (blue) in the left panel and other examples for $\boldsymbol{p} = [\omega_0, \alpha_2, t_1, \phi_1]$ (black), $[\omega_0, \alpha_2, t_2, \phi_2]$ (red), and $[\omega_0, \alpha_2, t_3, \phi_3]$ (blue) in the right panel, where $\omega_0 = 2\pi$ rad/s, $\alpha_1 = 0.3$, $\alpha_2 = 0.5$, $\alpha_3 = 0.7$, $t_1 = 0.1$ s, $t_2 = 0.2$ s, $t_3 = 0.3$ s, $\phi_1 = 20°$, $\phi_2 = 40°$, $\phi_3 = 60°$.

where $g_0 > 0$ is selected so that $\max_t |g_{\boldsymbol{p}}(t)| = 1$. The parameter vector $\boldsymbol{p}$ is defined as $\boldsymbol{p} = [\omega, \alpha, t_0, \phi]$, where $\omega = 2\pi f$ is the angular frequency of the heart interbeat interval $T = 1/f$, t_0 is the time delay, α is related to the second harmonic amplitude, and ϕ is related to the phase of the second harmonic. Some example waveforms of the proposed model function are shown in Fig. 5.

Using the proposed model function $g_{\boldsymbol{p}}(t)$, we present a function $G(W)$ that takes a large value when the estimated impulse response $\hat{h}_{i,j}(t)$ is accurately expressed using $g_{\boldsymbol{p}}(t)$. We consider the optimization problem

$$\hat{e}_{i,j} = \min_{\boldsymbol{p}} e_{i,j}(\boldsymbol{p}), \tag{11}$$

where $e_{i,j}(\boldsymbol{p})$ is defined as

$$e_{i,j}(\boldsymbol{p}) = \sqrt{\frac{1}{T} \int_{-T/2}^{T/2} |h_{i,j}(t) - g_{\boldsymbol{p}}(t)|^2 \, \mathrm{d}t}, \tag{12}$$

in which T is an observation time and $h_{i,j}(t)$ is normalized so that $\max_t |h_{i,j}(t)| = 1$. Note that $e_{i,j}(\boldsymbol{p})$ is the root-mean-square (rms) error between the impulse response $h_{i,j}(t)$ and the model function $g_{\boldsymbol{p}}(t)$ when the parameter $\boldsymbol{p}$ is optimized. Thus, the difference between the impulse response and the optimized model function can be evaluated using $\hat{e}_{i,j}$. Based on these factors, we propose a function $G(W)$ as

$$G(W) = \prod_{1 \le i < j \le M} \sigma(-c_1 \hat{e}_{i,j} + c_2), \tag{13}$$

where c_1, c_2 are positive constants and $\sigma(\cdot)$ is the sigmoid function $\sigma(x) = \mathrm{e}^x/(\mathrm{e}^x + 1)$. The objective function is designed to return larger values when the measured impulse response is more accurately approximated by the model function.

Finally, the proposed blind signal separation method is formulated as the following optimization problem:

$$\max_W F'(W) = F_1(W) F_2(W) G(W). \tag{14}$$

The performance of this method is experimentally evaluated in the next section.

4. Performance Evaluation of the Proposed Blind Signal Separation Method

4.1 Experimental Setup

We performed measurements with two participants using an array radar system and a pair of laser displacement sensors. The array radar system is a frequency-modulated continuous wave (FMCW) radar with a center frequency of 79 GHz, center wavelength of $\lambda = 3.8$ mm, and frequency bandwidth of 3.9 GHz. The beamwidths of the antenna element pattern are ±4° and ±35° in the E- and H-planes, respectively. The radar has a multiple-input multiple-output (MIMO) array with three transmitting and four receiving elements; the spacings between the transmitting elements and between the receiving elements are 2λ and $\lambda/2$, respectively. When the distance to the target is sufficiently larger than the array aperture size, the MIMO array can be approximated using a virtual array. That is, the array of the radar system can be approximated using a 12-element virtual linear array with half-wavelength element spacings, which corresponds to $N = 12$ (see Sect. 2). The radar pulse repetition frequency was set to 10 Hz and the observation time was $T = 5$ s.

During the measurements, the participants were instructed to remain still in a prone position on a styrofoam bed while holding their breath. We set the coordinate system as shown in Fig. 1. The top of the bed is parallel to the x-axis and placed at a distance of 1.2 m from the array baseline (x-axis). A pair of laser displacement sensors were installed 150 mm from the back and the calf of each participant. Note that the laser displacement sensors were only used to evaluate the accuracy of the radar-based displacement measurement. Fig. 2 shows the experimental setup with the array radar system and laser displacement sensors. Fig. 6 shows an example of the time-range profile of the radar echo power, where the DC component is suppressed to display a time-varying component. In the figure, we see a strong echo at a range of 1.2–1.3 m.

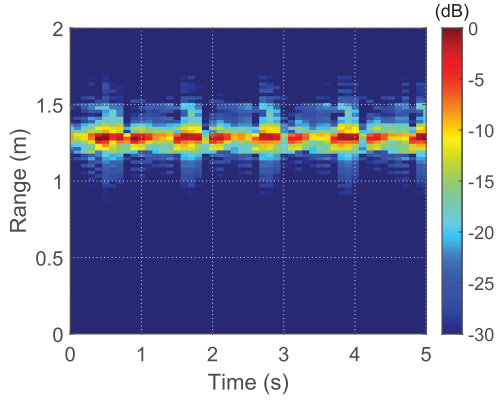

Fig. 6 Time-range profile of radar echo from a participant lying 1.2 m from the radar.

4.2 Application of Conventional and Proposed Blind Signal Separation Methods

We apply the conventional and proposed methods to the radar data measured from participants A and B, and evaluate their respective accuracy using the reference data measured by the laser displacement sensors. As conventional methods, we apply the BF and PHCA methods.

First, we apply the BF method to the data; this method was also used in our previous study [29]. The directions of arrival (DOAs) are estimated from the largest and second-largest peaks of the angular spectrum $P(\theta) = |\boldsymbol{w}^{\mathrm{H}}(\theta)\Lambda\boldsymbol{x}(t)|^2$, where $\boldsymbol{w}(\theta) = [w_1(\theta), \cdots, w_M(\theta)]^{\mathrm{T}}$, $w_m(\theta) = \mathrm{e}^{\mathrm{j}\pi m \sin\theta}$, and Λ is a diagonal matrix whose elements are the Taylor window coefficients. The estimated DOAs were $\theta_1 = -23.9°, \theta_2 = 5.4°$ for participant A. The angles θ_1 and θ_2 correspond to $x = 0.53$ m and $x = -0.11$ m, respectively. Considering the position and posture of the participant, θ_1 and θ_2 are interpreted as the DOAs of the back and calf of the participant. Similarly, for participant B, the DOAs were estimated as $\theta_1 = -25.1°, \theta_2 = 9.6°$, which correspond to $x = 0.56$ m and $x = -0.20$ m, respectively. For each participant, the echoes from DOAs $\theta = \theta_1$ and θ_2 were estimated as $\hat{s}_1(t) = \boldsymbol{w}^{\mathrm{H}}(\theta_1)\boldsymbol{x}(t)$ and $\hat{s}_2(t) = \boldsymbol{w}^{\mathrm{H}}(\theta_2)\boldsymbol{x}(t)$. The estimated displacement waveforms $\hat{d}_1(t) = (1/2k)\angle\hat{s}_1(t)$ and $\hat{d}_2(t) = (1/2k)\angle\hat{s}_2(t)$ are shown in Fig. 7, and the impulse responses $\hat{h}_{1,2}(t)$ are shown in Fig. 8.

Next, we applied PHCA to the measured data. We set $\beta = 2$, $\gamma = 0.1$, $c_1 = 2$, and $c_2 = 1$. Because PHCA separates signals by optimizing the objective function $\max_W F(W) = F_1(W)F_2(W)F_3(W)F_4(W)$, an optimization algorithm is required. As the optimization algorithm, we adopted an island-model real-coded genetic algorithm, with 100 individuals on each of eight islands, 50 generations, and genes consisting of 12×2 matrices in which all elements are initially set to 1. The waveforms $\hat{d}_1(t)$ and $\hat{d}_2(t)$ of both participants are shown in Fig. 9, and the estimated

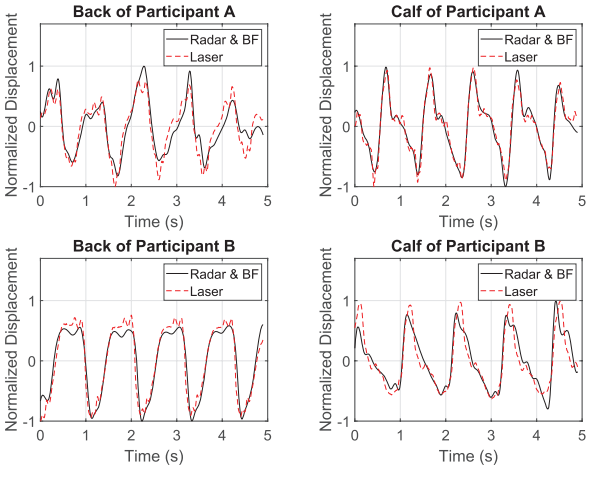

Fig. 7 Displacements estimated using the radar and BF method (black) and the laser displacement sensor (red dashed) for participants A and B.

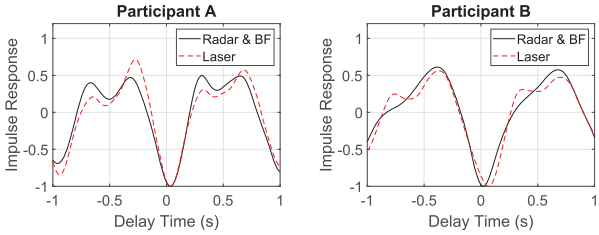

Fig. 8 Impulse response calculated from the pulse waveform estimated using the BF method (black line) and the impulse response calculated from the pulse wave waveform measured by the laser displacement sensor (red dashed line). Left: participant A; right: participant B.

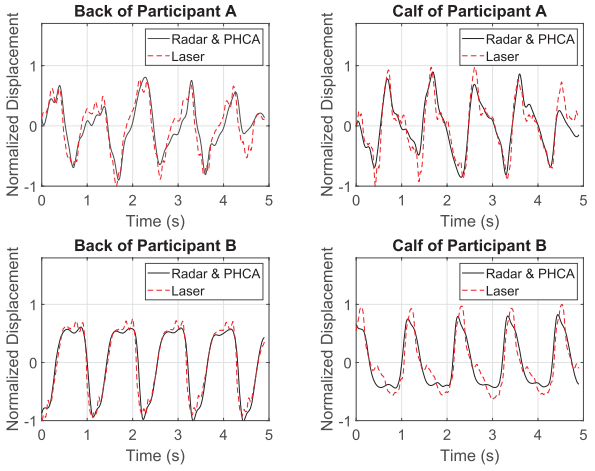

Fig. 9 Displacement waveforms estimated using the radar and PHCA (black) and reference data measured using laser displacement sensors (red dashed).

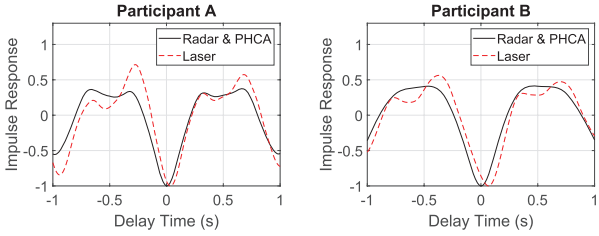

Fig. 10 Impulse response (black) estimated using PHCA for participants A (left) and B (right) with reference data (red dashed).

impulse responses $\hat{h}_{1,2}(t)$ are shown in Fig. 10.

Finally, we applied the proposed method to the measured data. The parameters were set to be the same as those for PHCA. The objective function of PHCA, $F(W)$, was replaced by $F'(W) = F_1(W)F_2(W)G(W)$. The displacement waveforms $\hat{d}_1(t)$ and $\hat{d}_2(t)$ were estimated using the proposed method. The results are displayed in Fig. 11, and the impulse responses $\hat{h}_{1,2}(t)$ are shown in Fig. 12.

To evaluate the performance of the signal separation methods, we use two types of errors: (1) the rms error e_d in estimating the body displacement waveform and (2) the rms error e_imp in estimating the impulse response of the pulse wave. We define e_d and e_imp as

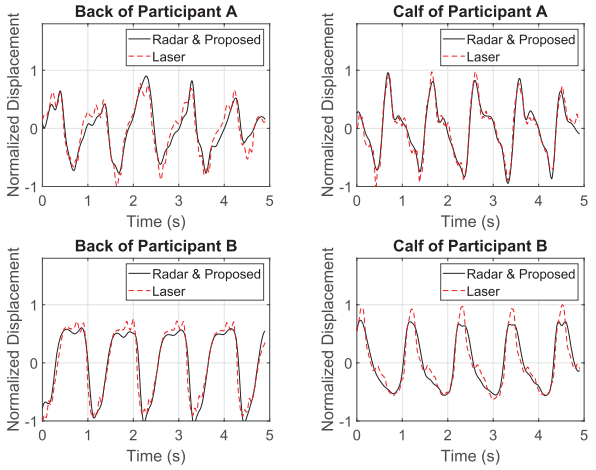

Fig. 11 Displacement waveforms estimated using the radar and proposed method (black) and reference data measured using laser displacement sensors (red dashed).

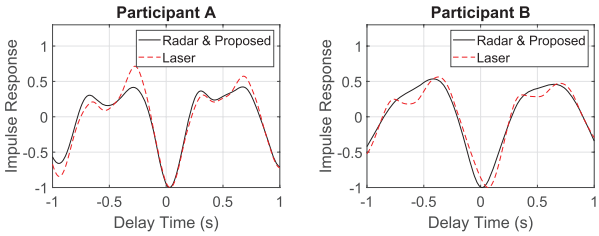

Fig. 12 Impulse response (black) estimated using the proposed method for participants A (left) and B (right) with reference data (red dashed).

$$e_\mathrm{d}(i) = \min_a \sqrt{\frac{1}{T}\int_0^T |a\hat{d}_i(t) - d_i(t)|^2\,\mathrm{d}t}, \tag{15}$$

$$e_\mathrm{imp} = \min_a \sqrt{\frac{1}{T}\int_{-T/2}^{T/2} |a\hat{h}_{1,2}(t) - h_{1,2}(t)|^2\,\mathrm{d}t}. \tag{16}$$

The rms errors $e_\mathrm{d}(1)$, $e_\mathrm{d}(2)$, $\bar{e}_\mathrm{d} = (e_\mathrm{d}(1) + e_\mathrm{d}(2))/2$, and e_imp are summarized in Table 3. In estimating the displacements at the back and calf of participant A, the proposed method achieves higher average accuracy than BF and PHCA (by 10% and 47%, respectively); in estimating the impulse response of the pulse wave in participant A, the proposed method is 26% and 71% more accurate than BF and PHCA, respectively. In estimating the displacements at the back and calf of participant B, the proposed method achieves 12% higher average accuracy than BF, and almost equivalent accuracy to that of PHCA; in estimating the impulse response of the pulse wave in participant B, the proposed method gives 28% higher accuracy than PHCA, and a similar level of accuracy as BF. Using the proposed method, the average error $\bar{e}_\mathrm{d}$ in estimating the displacement waveforms decreases by 10% (participant A) and 12% (participant B) compared with the BF method, and by 47% (participant A) compared with PHCA.

Finally, we estimated the PTT values (t_PTT) from the impulse responses $\hat{h}_{1,2}(t)$ obtained using PHCA and the pro-

Table 3 Accuracy of signal separation methods.

Method	Subject	Back $e_{\mathrm{d}}(1)$	Calf $e_{\mathrm{d}}(2)$	Ave. $\bar{e}_{\mathrm{d}}$	Imp. Res. e_{imp}
BF	A	0.18	0.10	0.14	0.14
	B	0.16	0.19	0.17	0.09
PHCA	A	0.19	0.19	0.19	0.19
	B	0.15	0.16	0.15	0.12
Proposed	A	0.16	0.10	0.13	0.11
	B	0.157	0.15	0.15	0.09

Table 4 Comparison of estimated PTT values.

	Participant A		Participant B	
	PTT	Error	PTT	Error
Laser	45.0 ms	–	35.5 ms	–
PHCA	5.3 ms	39.7 ms (88%)	−5.0 ms	40.5 ms (114%)
Proposed	30.5 ms	14.5 ms (32%)	33.0 ms	2.5 ms (7%)

posed method for comparison. The estimated PTT values were calculated as $t_{\mathrm{PTT}} = (t_{\mathrm{zero}}^{(-)} + t_{\mathrm{zero}}^{(+)})/2$, where $t_{\mathrm{zero}}^{(-)}$ and $t_{\mathrm{zero}}^{(+)}$ are the zero-crossing points that satisfy $\hat{h}_{1,2}(t_{\mathrm{zero}}^{(-)}) = \hat{h}_{1,2}(t_{\mathrm{zero}}^{(+)}) = 0$, $t_{\mathrm{zero}}^{(-)} < 0 < t_{\mathrm{zero}}^{(+)}$, and $|t_{\mathrm{zero}}^{(-)}|, |t_{\mathrm{zero}}^{(+)}| \leq t_{\mathrm{zero}}^{\max}$, where $t_{\mathrm{zero}}^{\max} = 0.5$ was selected. The estimated PTT values are summarized in Table 4. These results suggest that the accuracy can be significantly improved by using the proposed method instead of the original PHCA. Overall, the results indicate the effectiveness of the proposed method in measuring the body displacements at multiple body positions.

Note that, before applying the signal separation methods, the DC components were subtracted from $\boldsymbol{x}(t)$ to suppress static clutter, such as echoes from static objects (e.g., floor and bed) and non-moving body parts. Because the participants were holding their breath during the measurement, the radar signal mainly contained the displacement caused by pulse waves. The amplitude of the body displacement caused by the pulse waves varies across the body—the upper torso exhibits a large displacement because it is close to the heart, and the calves also exhibit a large displacement because they have a relatively large artery (i.e., popliteal artery and tibioperoneal trunk) located just beneath the skin. Experimentally, we have confirmed that strong radar echoes arrive mainly from these two positions (back and calf) when the target person is prone and the radar is installed above the body.

5. Conclusion

This paper has proposed a new method of blind signal separation and described the application of the method to the measurement of radar echoes from multiple body positions, allowing arterial pulse wave propagation to be observed. First, we measured the skin displacement on the backs and calves of two participants using laser displacement sensors, and proposed a mathematical model of the pulse wave propagation between the two body positions. The mathematical model was incorporated into a function that indicates the similarity between the mathematical model and the actual data. The objective function of conventional PHCA was then revised using the function formulated by the proposed mathematical model.

To evaluate the accuracy of the proposed method, we performed radar measurements on two participants. Compared with conventional methods, the proposed approach is better able to separate radar echoes accurately, with a few exceptions. The rms error of the proposed method in estimating the displacement waveforms was found to be 10% and 21% smaller than that of the conventional BF and PHCA methods, respectively. The rms error of the proposed method in estimating the impulse response of the pulse wave was found to be 15% and 55% smaller than that of the conventional BF and PHCA methods, respectively.

These results indicate that the proposed method is effective for the signal separation of radar echoes from multiple body positions. The blind signal separation method proposed in this study is expected to lead to new mathematical models of physiological signals being exploited to improve the measurement performance. We plan to establish other mathematical models of physiological signals so that similar approaches can be applied to other physiological measurements.

Acknowledgments

This work was supported in part by SECOM Science and Technology Foundation, JSPS 19H02155 and 21H03427, JST JPMJPR1873, and JST COI JPMJCE1307. The author thanks Mr. Takehito Koshisaka and Mr. Yuji Oyamada of Kyoto University for their help with this study. The author also thanks Dr. Hirofumi Taki and Dr. Shigeaki Okumura of MaRI Co., Ltd. for their technical advice. Finally, I would like to thank Stuart Jenkinson, PhD, from Edanz for editing a draft of this manuscript.

Ethics Declarations

This study was approved by the Ethics Committee of the Graduate School of Engineering, Kyoto University (permit no. 201916). Informed consent was obtained from all participants in the study.

References

[1] National Center for Health Statistics, "Summary health statistics: National health interview survey, 2018, Table A-1b, A-1c," http://ftp.cdc.gov/pub/Health_Statistics/NCHS/NHIS/SHS/2018_SHS_Table_A-1.pdf, accessed Jan. 7, 2022.

[2] J. Blacher, A.P. Guerin, B. Pannier, S.J. Marchais, M.E. Safar, and G.M. London, "Impact of aortic stiffness on survival in end-stage renal disease," Circulation, vol.99, no.18, pp.2434–2439, May 1999. DOI: 10.1161/01.cir.99.18.2434.

[3] S. Laurent, B. Kingwell, A. Bank, M. Weber, and H. Struijker-Boudier, "Clinical applications of arterial stiffness: Therapeutics and pharmacology," Am. J. Hypertens., vol.15, no.5, pp.453–458, May 2002. DOI: 10.1016/s0895-7061(01)02329-9.

[4] S. Meaume, A. Benetos, O.F. Henry, A. Rudnichi, and M.E. Safar,

"Aortic pulse wave velocity predicts cardiovascular mortality in subjects > 70 years of age," Arterioscler. Thromb. Vasc. Biol., vol.21, no.12, pp.2046–2050, Dec. 2001.

[5] S.S. Najjar, A. Scuteri, V. Shetty, J.G. Wright, D.C. Muller, J.L. Fleg, H.P. Spurgeon, L. Ferrucci, and E.G. Lakatta, "Pulse wave velocity is an independent predictor of the longitudinal increase in systolic blood pressure and of incident hypertension in the Baltimore longitudinal study of aging," J. Am. Coll. Cardiol., vol.51, no.14, pp.1377–1383, Nov. 2009. DOI: 10.1016/j.jacc.2007.10.065.

[6] J. Topouchian, R. El Feghali, B. Pannier, S. Wang, F. Zhao, K. Smetana, K. Teo, and R. Asmar, "Arterial stiffness and pharmacological interventions-the TRanscend arterial stiffness substudy (TRANS study)," Vasc. Health Risk Manag., vol.3, no.4, pp.381–387, Aug. 2007.

[7] R.A. Payne, C.N. Symeonides, D.J. Webb, and S.R.J. Maxwell, "Pulse transit time measured from the ECG: An unreliable marker of beat-to-beat blood pressure," J. Appl. Physiol., vol.100, no.1, pp.136–141, Jan. 2006. DOI: 10.1152/japplphysiol.00657.2005.

[8] R. Mukkamala, J.-O. Hahn, O.T. Inan, L.K. Mestha, C.-S. Kim, H. Toreyin, and S. Kyal, "Toward ubiquitous blood pressure monitoring via pulse transit time: Theory and practice," IEEE Trans. Biomed. Eng., vol.62, no.8, pp.1879–1901, Aug. 2015. DOI: 10.1109/TBME.2015.2441951.

[9] M. O'Rourke, W.W. Nichols, and C. Vlachopoulos, McDonald's Blood Flow in Arteries: Theoretical, Experimental and Clinical Principles, 6th ed., CRC Press, Boca Raton, FL, USA, 2011.

[10] J. Lass, K. Meigas, D. Karai, R. Kattai, J. Kaik, and M. Rossmann, "Continuous blood pressure monitoring during exercise using pulse wave transit time measurement," Proc. 26th Ann. Int. Conf. IEEE EMBS, San Francisco, CA, USA, pp.2239–2242, 2004. DOI: 10.1109/IEMBS.2004.1403652.

[11] T. Ma and Y. Zhang, "A correlation study on the variabilities in pulse transit time, blood pressure, and heart rate recorded simultaneously from healthy subjects," Proc. 27th Ann. Conf. IEEE Eng. Med. Biology, Shanghai, China, pp.996–999, Jan. 2005. DOI: 10.1109/IEMBS.2005.1616585.

[12] M.Y.-M. Wong, C.C.-Y. Poon, and Y.-T. Zhang, "An evaluation of the cuffless blood pressure estimation based on pulse transit time technique: A half year study on normotensive subjects," Cardiovasc. Eng., vol.9, no.1, pp.32–38, March 2009. DOI: 10.1007/s10558-009-9070-7.

[13] Y. Zheng, B.P. Yan, Y. Zhang, C.M. Yu, and C.C. Y. Poon, "Wearable cuff-less PTT-based system for overnight blood pressure monitoring," Proc. 35th Ann. Int. Conf. IEEE EMBS, Osaka, Japan, pp.6103–6106, 2013. DOI: 10.1109/EMBC.2013.6610945.

[14] S.S. Thomas, V. Nathan, C. Zong, K. Soundarapandian, X. Shi, and R. Jafari, "BioWatch: A noninvasive wrist-based blood pressure monitor that incorporates training techniques for posture and subject variability," IEEE J. Biomed. Health Inform., vol.20, no.5, pp.1291–1300, Sept. 2016. DOI: 10.1109/JBHI.2015.2458779.

[15] Y. Zheng, C.C.Y. Poon, B.P. Yan, and J.Y.W. Lau, "Pulse arrival time based cuff-less and 24-h wearable blood pressure monitoring and its diagnostic value in hypertension," J. Med. Syst., vol.40, art. no.195, 2016. DOI: 10.1007/s10916-016-0558-6.

[16] D.B. McCombie, A.T. Reisner, and H.H. Asada, "Adaptive blood pressure estimation from wearable PPG sensors using peripheral artery pulse wave velocity measurements and multi-channel blind identification of local arterial dynamics," Proc. 2006 Int. Conf. IEEE Eng. Med. Biol. Soc., New York, pp.3521–3524, 2006.

[17] Y. Hsu and D.J. Young, "Skin-coupled personal wearable ambulatory pulse wave velocity monitoring system using microelectromechanical sensors," IEEE Sensors J., vol.14, no.10, pp.3490–3497, Oct. 2014. DOI: 10.1109/JSEN.2014.2345779.

[18] C. Holz and E.J. Wang, "Glabella: Continuously sensing blood pressure behavior using an unobtrusive wearable device," Proc. ACM Interact. Mob. Wearable Ubiquitous Technol., vol.1, no.1, art. no.58, pp.1–23, Sept. 2017. DOI: 10.1145/3132024.

[19] Y.-J. Lee, C.-K. Lee, M. Kang, S.-J. Kang, K.-N. Kim, K. Kim, K.-S. Kim, and J.-W. Lee, "Magneto-plethysmographic sensor for peripheral blood flow velocity," IEEE Sensors J., vol.14, no.5, pp.1341–1342, May 2014. DOI: 10.1109/JSEN.2014.2304752.

[20] F. Heydari, M.P. Ebrahim, T. Wu, K. Walker, K. Joe, J.-M. Redoute, and M.R. Yuce, "Continuous cuffless blood pressure measurement using body sensors," 2018 IEEE Sensors Conf., New Delhi, India, 2018. DOI: 10.1109/ICSENS.2018.8630294.

[21] S.L.-O. Martin, A.M. Carek, C.-S. Kim, H. Ashouri, O.T. Inan, J.-O. Hahn, and R. Mukkamala, "Weighing scale-based pulse transit time is a superior marker of blood pressure than conventional pulse arrival time," Sci. Rep., vol.6, art. no.39273, 2016. DOI: 10.1038/srep39273.

[22] D. Buxi, J.M. Redouté, and M.R. Yuce, "Cuffless blood pressure estimation from the carotid pulse arrival time using continuous wave radar," Proc. 37th Annu. Int. Conf. IEEE EMBS, Milan, Italy, pp.5704–5707, 2015. DOI: 10.1109/EMBC.2015.7319687.

[23] D. Buxi, J. Redouté, and M.R. Yuce, "Blood pressure estimation using pulse transit time from bioimpedance and continuous wave radar," IEEE Trans. Biomed. Eng., vol.64, no.4, pp.917–927, April 2017. DOI: 10.1109/TBME.2016.2582472.

[24] M.P. Ebrahim, F. Heydari, T. Wu, K. Walker, K. Joe, J.-M. Redoute, and M.R. Yuce, "Blood pressure estimation using on-body continuous wave radar and photoplethysmogram in various posture and exercise conditions," Sci. Rep., vol.9, art. no.16346, 2019. DOI: 10.1038/s41598-019-52710-8.

[25] M. Kuwahara, E. Yavari, and O. Boric-Lubecke, "Non-invasive, continuous, pulse pressure monitoring method," Proc. Annu. Int. Conf. IEEE EMBS, Berlin, Germany, pp.6574–6577, July 2019. DOI: 10.1109/EMBC.2019.8857439.

[26] L. Lu, C. Li, and D.Y.C. Lie, "Experimental demonstration of noncontact pulse wave velocity monitoring using multiple Doppler radar sensors," Proc. 2010 Annu. Int. Conf. IEEE Eng. Med. Biol., Buenos Aires, Argentina, pp.5010–5013, Aug. 2010. DOI: 10.1109/IEMBS.2010.5627213.

[27] F. Michler, K. Shi, S. Schellenberger, B. Scheiner, F. Lurz, R. Weigel, and A. Koelpin, "Pulse wave velocity detection using a 24-GHz six-port based Doppler radar," 2019 IEEE Radio Wirel. Symp., Orlando, FL, USA, Jan. 2019. DOI: 10.1109/RWS.2019.8714521.

[28] R. Vasireddy, J. Goette, M. Jacomet, and A. Vogt, "Estimation of arterial pulse wave velocity from Doppler radar measurements: A feasibility study," 41st Annu. Int. Conf. IEEE EMBS, Berlin, Germany, pp.5460–5464, July 2019. DOI: 10.1109/EMBC.2019.8857644.

[29] Y. Oyamada, T. Koshisaka, and T. Sakamoto, "Experimental demonstration of accurate noncontact measurement of arterial pulse wave displacements using 79-GHz array radar," IEEE Sensors J., vol.21, no.7, pp.9128–9137, 2021. DOI: 10.1109/JSEN.2021.3052602.

[30] T. Sakamoto, "Signal separation using a mathematical model of physiological signals for the measurement of heart pulse wave propagation with array radar," IEEE Access, vol.8, pp.175921–175931, 2020. DOI: 10.1109/ACCESS.2020.3026539.

Takuya Sakamoto received a B.E. degree in electrical and electronic engineering from Kyoto University, Kyoto, Japan, in 2000, and M.I. and Ph.D. degrees in communications and computer engineering from the Graduate School of Informatics, Kyoto University, in 2002 and 2005, respectively. From 2006 to 2015, he was an Assistant Professor at the Graduate School of Informatics, Kyoto University. From 2011 to 2013, he was also a Visiting Researcher at Delft University of Technology, Delft, The Netherlands. From 2015 to 2018, he was an Associate Professor at the Graduate School of Engineering, University of Hyogo, Himeji, Japan. In 2017, he was also a Visiting Scholar at the University of Hawaii at Manoa, Honolulu, HI, USA. Since 2018, he has been a PRESTO Researcher at the Japan Science and Technology Agency, Kawaguchi, Japan. At present, he is an Associate Professor at the Graduate School of Engineering, Kyoto University. His current research interests are system theory, inverse problems, radar signal processing, radar imaging, and wireless sensing of vital signs. Dr. Sakamoto was a recipient of the Best Paper Award from the International Symposium on Antennas and Propagation (ISAP) in 2012, and the Masao Horiba Award in 2016. In 2017, he was invited as a semi-plenary speaker to the European Conference on Antennas and Propagation (EuCAP) in Paris, France.